# CRISPR screening identifies GNPTAB as a noncanonical STING activator driving cellular senescence

## Supplemental materials

### Method

### Cell culture

Human mesenchymal progenitor cells (hMPCs) were differentiated from human embryonic stem cells (hESCs) as previously described (Wu et al., 2018; Zhang et al., 2015). hMPCs were cultured on 0.1% gelatin-precoated plates (CORNING, 3516) in α-MEM (Gibco, 32571101) supplemented with 10% heat-inactivated fetal bovine serum (Gemini, A33H00K), 1× GlutaMAX (Gibco, 35050061), 0.1 mM non-essential amino acids (NEAA, Gibco, 11140076), 1× penicillin-streptomycin (Gibco, 15140122), 2.5 μg/mL plasmocin (InvivoGen, ant-mpt), and 1 ng/mL recombinant human bFGF (PeproTech, 450-33). Cells were maintained at 37 °C with 5% $CO_2$ in a humidified incubator, with medium refreshed every 2 days. When reaching 80-90% confluency, cells were rinsed twice with pre-warmed PBS, detached with TrypLE Express (Gibco, 12604021) at 37 °C for 3-5 min, neutralized with complete medium, centrifuged at 1,000 rpm for 5 min. EP hMPC refers to cells at passages 3-5 (P3-P5), while LP hMPC refers to cells at P13-P15.

The differentiation potential of hMPCs was assessed as described previously (Wang et al., 2021), with their adipogenic, chondrogenic, and osteogenic differentiation capacities evaluated by the Oil Red O staining (Sigma-Aldrich, O1391), Alcian blue staining (Solarbio, G3668-100), and von Kossa staining (GENMED, GMS 80045.3) respectively.

### Plasmid construction

The 3×Flag-tagged GNPTAB plasmid was amplified from hMPC-derived cDNA and cloned into the pLE4 vector (a kind gift from Dr. Tomoaki Hishida) using the NovoRec® Plus One-Step Cloning Kit (Novoprotein, NR005B). GNPTAB-E937K, GNPTAB-K952A, GNPTAB-E1119A, GNPTAB-R1127A, and GNPTAB-Q1136A mutant plasmids were constructed with the Fast Mutagenesis System (TRANS, FM111-01).

For lentivirus-mediated CRISPR knockout (CRISPRko), single guide RNAs (sgRNAs) targeting *GNPTAB* were cloned into the lentiCRISPRv2 plasmid (Addgene #52961) as previously described (Li et al., 2023). Primer sequences are listed in Table S6.

### Lentiviral production

Lentiviruses were produced as previously reported (Li et al., 2024). Briefly, HEK 293T cells were co-transfected with the target plasmid, packaging plasmid psPAX2 (Addgene, Cat# 12260), and envelope plasmid pMD2.G (Addgene, Cat# 12259) using Lipofectamine 3000 (Thermo Fisher Scientific, L3000015). Viral supernatants were collected at 24, 48, and 72 h post-transfection, filtered through a 0.45 μm membrane, and ultracentrifuged at 19,400 rpm for 2 h at 4 °C. The pellets were resuspended in PBS and stored at -80 °C.

**CRISPR/Cas9 loss-of-function (LOF) screening for lysosome-associated genes (LAGs) in hMPCs**

A custom sgRNA library targeting 148 LAGs was designed by selecting three independent sgRNAs per gene from a genome-wide knockout library (sequences listed in Table S1), resulting in a total of 454 sgRNAs (Sanjana et al., 2014). The library was constructed as previously described (Li et al., 2024). Briefly, all sgRNAs were cloned into the lentiCRISPRv2 vector (Joung et al., 2017; Li et al., 2023). Individual plasmids were verified by Sanger sequencing to confirm correct sgRNA insertion, and the final sgRNA library was prepared by pooling equimolar amounts of each verified plasmid. Library representation was confirmed by next-generation sequencing of the plasmid pool. Generally, a qualified CRISPR screening library requires the percentage of guides that match perfectly to exceed 70%, the percentage of mapped reads to be greater than 65%, and the mapped reads per sgRNA to exceed 300 (Joung et al., 2017; Li et al., 2015; Wang et al., 2019).

The screen was performed in three independent biological replicates. Senescent hMPCs were seeded into 15 cm dishes at a density of $1 \times 10^6$ cells per dish and cultured overnight. The next day, cells were infected with the concentrated lentivirus harboring LAGs sgRNA library at a multiplicity of infection (MOI) of approximately 0.3 in the presence of polybrene to ensure that the vast majority of cells received at most one sgRNA, while maintaining a library coverage of >500x. Cells transduced with non-targeting control (NTC) sgRNA were used as the negative control. At 48 h post-infection, cells were subjected to puromycin selection (1 μg/mL) (InvivoGen) for 6 consecutive days to eliminate non-transduced cells. Subsequently, the selected cells were maintained in antibiotic-free medium and passaged every 3-4 days until sgNTC-transduced cells exhibited obvious proliferative arrest.

At the terminal point of screening, genomic DNA (gDNA) was extracted from at least $1 \times 10^6$ cells per sample using the TIANamp Genomic DNA Kit (TIANGEN, DP304-03) according to the manufacturer's instructions. The sgRNA sequence was amplified by two-step PCR using PrimeSTAR® HS DNA Polymerase (Takara Bio, R044A) followed by next-generation sequencing (NGS) on the Illumina NovaSeq 6000 platform (Illumina) (Jing et al., 2023).

**Western blotting**

Western blotting was performed as previously reported (Wang et al., 2021). Briefly, cells were lysed in 1× SDS lysis buffer (62.5 mM Tris-HCl pH 6.8, 2% SDS) and boiled at 105 °C for 10 min. Protein concentrations were quantified using the BCA assay (Dingguo, BCA-02). Equal amounts of protein (20 μg) were separated by SDS–PAGE and transferred onto PVDF membranes (Millipore, ISEQ00010). Membranes were blocked with 5% non-fat milk in TBST at room temperature for 1 h, then incubated with primary antibodies overnight at 4 °C, followed by HRP-conjugated secondary antibodies for 1 h. Signals were visualized using the ChemiDoc XRS+ system (Bio-Rad) and quantified with ImageJ software.

The levels of procathepsin B in the cell culture medium were determined by collecting the entire culture medium and counting the cell number at 24 h after cell passage. The medium was centrifuged at 4,500 rpm for 20 min using an ultrafiltration tube (Merck Millipore, UFC903096), and an equal volume of the supernatant was subjected to Western blot analysis. The data were normalized to the total cell number.

Primary antibodies: anti-GNPTAB (ABclonal, A15895), anti-Lamin B1 (Abcam, ab16048), anti-LAP2 (BD Bioscience, 611000), anti-P21 (Abcam, ab188224), anti-P16 (BD Bioscience, 550834), anti-STING (Cell Signaling Technology, 13647S), anti-Phospho-STING (Cell Signaling Technology, 19781S), anti-Phospho-TBK1 (Cell Signaling Technology, 5483S), anti-Phospho-IRF3 (Cell Signaling Technology, 29047S), anti-Phospho-NF-kappaB (Cell Signaling Technology, 3033S), anti-cathepsin B (Abcam, ab58802), anti-β-Actin (Santa Cruz, sc-69879), anti-β-Tubulin (Immunoway, YM3030), anti-GAPDH (ABclonal, A19056) and anti-Flag (Sigma-Aldrich, F1804).

Secondary antibodies: HRP-conjugated secondary antibodies are goat anti-mouse (ZSGB-BIO, ZB2305) and goat anti-rabbit (ZSGB-BIO, ZB2301).

**Clonal expansion analysis**

Clonal expansion analysis was performed as previously described (Zhang et al., 2022). Briefly, hMPCs were dissociated into single-cell suspension with TrypLE Express and seeded at 3,000 cells/well in 12-well plates. Cells were cultured for ~12 days, with medium refreshed every 2 days. Colonies were fixed with 4% paraformaldehyde (PFA, Dingguo, AR-0211) at room temperature for 15 min, stained with 0.1% crystal violet solution (Biohao, C0520) for 15 min at room temperature, and then rinsed thoroughly with sterile PBS to remove excess dye. Images were acquired using a flatbed scanner (Epson) and Olympus inverted microscope. The density was quantified with ImageJ software.

**Senescence-associated β-galactosidase (SA-β-Gal) staining**

SA-β-Gal staining was performed as previously described (Geng et al., 2023; Liu et al., 2011). Briefly, cells were rinsed twice with pre-warmed PBS, fixed in 2% formaldehyde/0.2% glutaraldehyde (Sigma-Aldrich, F8775) in PBS at room temperature for 5 min, and then washed three times with PBS to remove residual fixative. Cells were incubated overnight at 37 °C with SA-β-Gal staining solution (pH 6.0) containing 1 mg/mL X-gal (Solarbio, X1010-1), 40 mM citric acid/sodium phosphate buffer (SCR, 10007192), 5 mM potassium ferrocyanide (SCR, 10016718), 5 mM potassium ferricyanide (SCR, 10016818), 150 mM NaCl (SCR, 10019318), and 2 mM $MgCl_2$ (SCR, 10012818). Images were acquired using an Olympus inverted light microscope, and SA-β-Gal-positive cells were quantified with ImageJ software.

**RNA extraction, reverse transcription, and RT-qPCR analysis**

Total RNA was extracted with TRIzol (Life technologies) following the manufacturer's instructions. For reverse transcription (RT), 1 μg of total RNA was converted to complementary DNA (cDNA) using the GoScript™ Reverse Transcription System (Promega). Real-time quantitative polymerase chain reaction (RT-qPCR) was performed on a QuantStudio™ Real-Time PCR System using THUNDERBIRD® SYBR® qPCR Mix (TOYOBO). *ACTB* and *GAPDH* were used as the housekeeping genes for normalization. Primer sequences are listed in Table S6.

**RNA interference**

To knock down *MB21D1* or *STING1* in EP hMPCs, we transfected *MB21D1* or *STING1* siRNAs and non-targeting siRNA into EP hMPCs using RNAi MAX reagent following the manufacturer's instructions. Briefly, 100 nM siRNAs and 9 μL Lipofectamine RNAi max reagent were pooled into one well of six-well plates. The siRNA sequences are listed in Table S6.

**Immunofluorescence staining**

Cells were seeded on gelatin-coated glass coverslips (Thermo Fisher, 12-541-000) and cultured to 80% confluency. Then, cells were rinsed twice with pre-warmed PBS, fixed with 4% PFA in PBS at room temperature for 15 min, and permeabilized with 0.4% Triton X-100 (Sigma, T9284) in PBS for 15 min at room temperature. After three washes with PBS, non-specific binding was blocked with blocking buffer (10% donkey serum) for 1 h at room temperature. Cells were then incubated with primary antibodies (diluted in blocking buffer) overnight at 4 °C, followed by three PBS washes and incubation with fluorophore-conjugated secondary antibodies (1:1000 dilution in PBS) for 1 h at room temperature in the dark. Nuclei were counterstained with 5 μg/mL Hoechst 33342 (Invitrogen, H3570) for 10 min at room temperature. Coverslips were mounted onto glass slides using anti-fade mounting medium (Vector, H-1000) and imaged with a Zeiss LSM900 confocal microscope.

Primary antibodies: anti-Ki67 (ZSGB-BIO, ZM0166), anti-γH2AX (Millipore, 05-636), anti-53BP1 (Bethyl Laboratories, A300-273A), anti-H3K9me3 (Abcam, ab8898), anti-LAP2 (BD Biosciences, 611000), anti-HP1α (Cell Signaling Technology, 2616S) and anti-LAMP2 (Santa Cruz, sc-18822).

Secondary antibodies: Alexa Fluor 488-conjugated donkey anti-mouse (Invitrogen, A21202), Alexa Fluor 488-conjugated donkey anti-rabbit (Invitrogen, A21206), Alexa Fluor 568-conjugated donkey anti-mouse (Invitrogen, A10037) and Alexa Fluor 568-conjugated donkey anti-rabbit (Invitrogen, A10042).

**Telomere length measurement**

The telomere length was analyzed as described previously (Zhang et al., 2019). Genomic DNA was extracted using TIANamp Genomic DNA Kit (TIANGEN, DP304). Telomere length was measured by quantitative real-time PCR (qPCR) on a Bio-Rad CFX384 Touch Real-Time PCR System using telomere-specific primers and a single-copy gene (*RPLP0*) as the internal reference. Primer sequences are listed in Table S6.

**Enzyme-linked immunosorbent assay (ELISA)**

Cells were lysed using RIPA lysis buffer (Beyotime, P0013B), followed by centrifugation at 600 × g for 20 min at 4 °C. The supernatant of the lysate was collected, and the cyclic guanosine monophosphate-adenosine monophosphate (2′3′-cGAMP) level was measured using an ELISA kit (Cayman Chemical, 501700) according to the manufacturer's instructions. The microplate was read at 450 nm using a Synergy H1 microplate reader (BioTek), and the data were finally normalized to the total cell number.

**Cathepsin B (CTSB) enzymatic activity measurement**

For CTSB activity detection, cells were incubated with Magic Red™ Cathepsin B Fluorogenic Substrate (ICT-937) at 37 °C with 5% $CO_2$ for 15 min in the dark. After incubation, cells were fixed with 4% PFA in PBS at room temperature for 15 min, then washed three times with PBS. Nuclei were counterstained with Hoechst 33342 for 10 min at room temperature. Images were acquired using a Zeiss LSM900 confocal microscope, and relative CTSB activity was quantified as the mean fluorescence intensity of Magic Red signals per cell using ImageJ software.

**Lysosomal pH measurement**

Lysosomal pH was determined using the pHLys Red-Lysosomal acidic pH detection kit (DOJINDO, L265) following the manufacturer's protocol. Briefly, hMPCs were seeded into gelatin-precoated 24-well plates and cultured to 70-80% confluency. Cells were incubated with pHLys Red fluorescent probe (diluted in hMPC medium at a ratio of 1:1000) at 37 °C with 5% $CO_2$ for 15 min in the dark. After incubation, cells were gently rinsed twice with pre-warmed PBS, fixed with 4% PFA in PBS at room temperature for 15 min, and washed three times with PBS to remove residual fixative. Nuclei were counterstained with Hoechst 33342 for 10 min at room temperature in the dark. Images were acquired using a Zeiss LSM900 confocal microscope.

**CRISPR screening analysis**

Sequencing reads were processed to extract sgRNA sequences from FASTQ files and quantify their counts. Subsequent analysis was performed using MAGeCK (v0.5.9.5) (Li et al., 2014). The sgRNA counts were generated from each sample using the 'count' subcommand with default parameters, with high-quality reads aligned to the screening library. Differential enrichment of sgRNAs between experimental (3 replicates) and baseline conditions was assessed using the 'test' subcommand to identify positively and negatively selected sgRNAs, with parameters set as --remove-zero both. During analysis, sgRNAs with zero counts across all samples were removed. Significant sgRNAs were ranked and evaluated based on the robust rank aggregation (RRA) algorithm, with those showing $P$ value < 0.05 considered statistically significant and sorted by RRA score for positive selection (--sort-criteria pos).

**Bulk RNA-seq analysis**

Raw RNA-seq reads were quality-filtered and trimmed using Trim Galore (v0.6.10) to remove adapter sequences and low-quality bases (https://github.com/FelixKrueger/TrimGalore). The cleaned reads were then aligned to the human reference genome hg19 using STAR (v2.7.10b) (Dobin et al., 2013) with default parameters. Gene-level read counts were quantified with featureCounts (v2.1.1) (Liao et al., 2014).

Based on the resulting count matrix, differential expression analysis was performed using the R package DESeq2 (v1.38.3) (Love et al., 2014). Low-expressed genes (total counts ≤ 1) were filtered out, and data were normalized via rlog transformation. A negative binomial model was applied to test for expression differences. Significantly differentially expressed genes were defined as those with an adjusted $P$ value < 0.05 and $|\log_2(\text{Fold Change})| > 0.5$. Gene ontology (GO) terms and Kyoto Encyclopedia of Genes and Genomes (KEGG) pathways enrichment analyses for the identified significant genes were conducted using the Metascape (Zhou et al., 2019) online platform to uncover associated biological functions and pathways.

**Co-immunoprecipitation (Co-IP) and LC-MS/MS analysis**

Co-IP analysis was performed as described previously (He et al., 2023). HEK 293T cells were transfected with FLAG-tagged GNPTAB or Luc using Lipofectamine 3000. At 72 h post-transfection, cells were harvested and lysed in CHAPS lysis buffer (40 mM HEPES, pH 7.5, 120 mM NaCl, 0.3% CHAPS, 1 mM EDTA, 1 mM PMSF and complete protease inhibitor cocktail (Roche, 4693159001)) with gentle rotation at 4 °C for 2 h and clarified by centrifugation at 12,000

g at 4 °C for 30 min. An aliquot of each clarified lysate was saved as input control. The remaining supernatant was incubated with anti-Flag affinity gel (Sigma, A2220) overnight at 4 °C with rotation. The beads were then washed five times with lysis buffer to remove non-specifically bound proteins. Bound protein complexes were eluted with Flag peptide (Sigma, F3290) for 4 h at 4 °C, followed by boiling in SDS sample buffer. The input samples and immunoprecipitated complexes were resolved by Western blotting.

Proteins isolated via Co-IP were separated by sodium dodecyl sulfate-polyacrylamide gel electrophoresis (SDS-PAGE), followed by Coomassie Brilliant Blue staining. After destaining, gel bands containing the target protein were excised and subjected to a series of sample pretreatments: dehydration with 100% acetonitrile, reduction with 10 mM dithiothreitol (DTT) in 25 mM $NH_4HCO_3$ at 56 °C for 45 min, and alkylation with 10 mM iodoacetamide (IAM) in 25 mM $NH_4HCO_3$ at room temperature in the dark for 45 min. The processed gel pieces were then incubated with sequencing-grade modified trypsin (Worthington) in 25 mM $NH_4HCO_3$ at 37 °C overnight for enzymatic digestion. The reaction was terminated by adding formic acid, and the resulting peptide mixture was analyzed by nanoscale liquid chromatography coupled with Q Exactive mass spectrometry (nano-LC-Q EXACTIVE, Thermo Fisher Scientific) equipped with a nano-electrospray ionization (nano-ESI) source (Proxeon Biosystems). Raw mass spectrometry data were processed using MaxQuant software (version 1.3.0.5). The generated peak lists were further analyzed via Thermo Proteome Discoverer (version 1.4.0.288) against the UniProt human proteome database. For protein identification, the false discovery rate (FDR) was strictly controlled at 1% for both peptide and protein levels, with a minimum peptide length of 7 amino acids. Additionally, each identified protein was required to be matched with at least one unique or razor peptide.

Proteins that were detected exclusively in the GNPTAB group compared to the Luc group were considered candidate GNPTAB-interacting proteins. The complete list of GNPTAB-interacting proteins is listed in Table S5. To gain insights into the functional roles and cellular localization of these candidate proteins, biological process (BP) and cellular component (CC) analyses were performed using Metascape (Zhou et al., 2019).

**Protein docking**

The available experimentally resolved structures covering the relevant cytosolic and luminal domains were used for docking. The structures of STING (PDB ID: 4LOH) and GNPTAB (PDB ID: 7S05) were docked using the HDOCK server with default settings (Yan et al., 2017). Models were ranked based on docking and confidence scores, and the model that passed the threshold and had the highest confidence score was selected for analysis. Key residues involved in hydrogen bond formation were subsequently identified and analyzed using PyMOL 3.0.

**Molecular dynamics simulation**

All-atom molecular dynamics simulations were performed on the GNPTAB-WT-STING and GNPTAB-E1119A-STING complex models obtained from HDOCK docking. All simulations were carried out using GROMACS 2023.2 with the CHARMM36 force field. Each system was placed in a dodecahedral simulation box filled with TIP3P water molecules, with a minimum distance of 1.2 nm between the solute and the box boundary. To neutralize the systems and mimic physiological conditions, counterions were added and the salt concentration was adjusted to 0.15 M NaCl. Energy

minimization was first performed for 5000 steps using the steepest descent algorithm, followed by 500 ps equilibration in the NVT ensemble and 500 ps in the NPT ensemble to further relax the systems. Production simulations were then conducted at 300 K and 1 bar, with temperature and pressure controlled by the V-rescale thermostat and Parrinello-Rahman barostat, respectively. Long-range electrostatic interactions were treated with the particle-mesh Ewald (PME) method using a real-space cutoff of 1.2 nm, while van der Waals interactions were handled using a force-switch scheme that smoothly switched the interactions to zero between 1.0 and 1.2 nm. All bonds involving hydrogen atoms were constrained using the LINCS algorithm, and periodic boundary conditions were applied in all three spatial dimensions (x, y, and z). A time step of 2 fs was used, and trajectories were saved every 5 ps; each system was simulated for a total of 200 ns. Key conformational snapshots were visualized and analyzed using PyMOL 3.0 at the end of the simulations.

**Per-Residue Binding Free Energy Analysis**

The contribution of key GNPTAB residues involved in hydrogen bond formation to the binding free energy of the GNPTAB–STING complex was calculated using gmx_MMPBSA (v1.5.0.3) based on the Molecular Mechanics/Poisson–Boltzmann Surface Area (MM/PBSA) method (Valdés-Tresanco et al., 2021). After completion of the MD simulations, conformations were sampled from the production trajectory between frames 10,000 and 40,000 at 5 ps intervals, yielding a uniformly distributed set of structures for free energy analysis. The polar solvation energy was calculated using the Poisson–Boltzmann model with an ionic strength of 0.15 M and a grid scaling factor of 2.0, while all other parameters were kept at their default settings.

**Statistical analysis**

All senescence-related assays were performed with at least three independent biological replicates, each derived from independently prepared cell cultures. For SA-β-Gal staining, a minimum of 100 cells per replicate were counted from at least five randomly selected microscopic fields. For immunofluorescence quantification of Ki67, γH2A.X/53BP1 foci, Lamin B1, H3K9me3, LAP2, and HP1α, at least 100 cells per replicate were analyzed from a minimum of five fields, with all counts performed in a blinded manner. Co-localization was quantified using the Coloc plugin in Fiji, based on Manders' correlation coefficients (Liang et al., 2020). This parameter was defined as the fraction of STING fluorescence intensity within the Golgi matrix protein 130 (GM130)-positive region above threshold, relative to total cellular STING fluorescence intensity. A uniform threshold was used for all comparative analyses. Colony formation assays were conducted in triplicate wells per condition. Telomere length was measured by quantitative PCR in triplicate technical replicates for each biological sample. P16, P21, Lamin B1 and LAP2 protein levels were quantified by immunoblotting with densitometry normalized to loading control (β-Actin, β-Tubulin or GAPDH).

Data are presented as mean ± SEM. Statistical analyses were performed using GraphPad Prism (version 8). For comparisons between two groups, two-tailed Student's *t* test was employed if data conformed to a normal distribution, whereas two-tailed Wilcoxon test was used for non-normally distributed data. For comparisons among more than two groups, one-way analysis of variance (ANOVA) followed by Tukey's multiple-comparison test was applied if data were normally distributed; for non-normally distributed data, the nonparametric Kruskal-Wallis test with Dunn's multiple-comparison test was used instead. $P < 0.05$ was considered statistically significant.

**Supplemental figure legends**

**Figure S1: CRISPR/Cas9 screening identifies GNPTAB as a key regulator of human MPC senescence.**

(**A**) Clonal expansion analysis of EP and LP hMPCs.

(**B**) Immunofluorescence staining of Ki67 of EP and LP hMPCs. Scale bars, 20 μm. White arrows indicate Ki67-positive cells.

(**C**) SA-β-Gal staining of EP and LP hMPCs. Scale bars, 100 μm. Black arrows indicate SA-β-Gal-positive cells.

(**D**) Western blot analysis of P16, Lamin B1 and LAP2 protein levels in EP and LP hMPCs. GAPDH was used as the loading control.

(**E**) The quality control of LAGs sgRNA library.

(**F**) Bar plots showing the percentage of mapped reads at the baseline and terminal time points of the CRISPR screen in replicative senescence (RS) hMPCs. For the LAGs group, three biological replicates are shown and labeled as 1, 2 and 3.

(**G**) Bar plots showing the number of mapped reads per sgRNA at the baseline and terminal time points of the CRISPR screen in RS hMPCs. For the LAGs group, three biological replicates are shown and labeled as 1, 2 and 3.

(**H**) Heatmap showing the relative mRNA levels of *CDKN2A, CDKN1A, CXCL8, LMNB1* and *TMPO* in LP hMPCs after CRISPR-mediated knockout (CRISPRko) of *GNPTAB*. The color key represents relative expression levels.

**(I)** Immunofluorescence analysis of LAP2 in LP hMPCs after CRISPRko of *GNPTAB*. Scale bars, 20 μm.

(**J**) Immunofluorescence analysis of HP1α in LP hMPCs after CRISPRko of *GNPTAB*. Scale bars, 20 μm.

(**K**) Von kossa staining showing the osteogenesis potential of LP hMPCs after CRISPRko of *GNPTAB*. Scale bars, 100 μm.

(**L**) The relative diameters of chondrospheres showing the chondrogenesis capacity of LP hMPCs after CRISPRko of *GNPTAB*. Scale bars, 100 μm.

(**M**) Oil Red O staining showing the adipogenesis potential of LP hMPCs after CRISPRko of *GNPTAB*. Scale bars, 100 μm.

(**N**) Heatmap showing the Euclidean distances among individual samples of sg-*GNPTAB* and sg-*NTC*.

(**O**) Volcano plot showing the up-regulated (right) and down-regulated (left) differentially expressed genes (DEGs) in LP hMPCs after CRISPRko of *GNPTAB*.

(**P**) Heatmap showing the relative mRNA levels of *CDKN1A, IL1B, CXCL8, LMNB1* and *TMPO* in EP hMPCs transduced with lentiviruses expressing Luc or GNPTAB. The color key represents

relative expression levels.

(**Q**) The heatmap shows the Euclidean distances among individual samples of EP hMPCs transduced with lentiviruses expressing GNPTAB or Luc.

(**R**) Volcano plot showing the upregulated (right) and downregulated (left) differentially expressed genes (DEGs) in EP hMPCs transduced with lentiviruses expressing GNPTAB.

Data in all figures except for (E)-(H) and (N)-(R) are presented as mean ± SEM. Two-tailed unpaired Student's *t* test (A-D, K-M) and two-tailed Wilcoxon test (I, J) were used. $n$ = 3-4 biological replicates in (A)-(D), (K) and (M); $n \geq 300$ cells from three biological replicates in (I) and (J); $n$ = 7 biological replicates in (L).

**Figure S2: *GNPTAB* depletion attenuated hMPCs senescence.**

(**A**) Western blot analysis of GNPTAB protein level in Hutchinson-Gilford progeria syndrome (HGPS) hMPCs after CRISPRko of *GNPTAB*. β-Actin was used as the loading control.

(**B**) Clonal expansion analysis of HGPS hMPCs after CRISPRko *GNPTAB*.

(**C**) Immunofluorescence staining of Ki67 in HGPS hMPCs after CRISPRko of *GNPTAB*. Scale bars, 20 μm. White arrows indicate Ki67-positive cells.

(**D**) SA-β-Gal staining of HGPS hMPCs after CRISPRko of *GNPTAB*. Scale bars, 100 μm. Black arrows indicate SA-β-Gal-positive cells.

(**E**) Immunofluorescence analysis of H3K9me3 in HGPS hMPCs after CRISPRko of *GNPTAB*. Scale bars, 20 μm.

(**F**) Immunofluorescence analysis of LAP2 in HGPS hMPCs after CRISPRko of *GNPTAB*. Scale bars, 20 μm.

(**G**) qPCR analysis of telomere length in HGPS hMPCs after CRISPRko of *GNPTAB*. The expression level was normalized to *RPLP0*.

(**H**) Clonal expansion analysis of UV (ultraviolet)-induced senescence after CRISPRko of *GNPTAB*.

(**I**) Immunofluorescence analysis of Ki67 of UV-induced senescence after CRISPRko of *GNPTAB*. Scale bars, 20 μm. White arrows indicate Ki67-positive cells.

(**J**) SA-β-Gal staining of UV-induced senescence after CRISPRko of *GNPTAB*. Scale bars, 100 μm. Black arrows indicate SA-β-Gal-positive cells.

Data in all figures are presented as mean ± SEM. Two-tailed unpaired Student's *t* test (A-D, G), two-tailed Wilcoxon test (E, F) and one-way ANOVA followed by Tukey's multiple-comparison test (H-J) were used. $n$ = 3-4 biological replicates in (A)-(D) and (G)-(J); $n \geq 300$ cells from three biological replicates in (E); $n \geq 400$ cells from four biological replicates in (F).

**Figure S3: Activation of lysosomal activity and STING signaling during hMPCs senescence**

**(A)** Immunofluorescence staining of LAMP2 in EP and LP hMPCs. Scale bars, 20 μm.

**(B)** Immunofluorescence staining of pHLys Red in EP and LP hMPCs. Scale bars, 20 μm.

**(C)** Immunofluorescence staining of CTSB in EP and LP hMPCs. Scale bars, 20 μm.

**(D)** Colocalization and intensity profiles of Flag and STING in EP hMPCs transduced with lentiviruses expressing Flag-GNPTAB. Scale bars, 20 μm.

**(E)** Western blot analysis of procathepsin B protein levels in media of EP hMPCs transduced with lentiviruses expressing Luc, GNPTAB-WT or GNPTAB-E1119A. The procathepsin B protein levels were normalized to the content of 5E5 cells.

**(F)** Western blot analysis of p-STING, p-TBK1, p-IRF3 and p-NF-κB protein levels in EP and LP hMPCs. β-Tubulin was used as the loading control.

**(G)** Relative mRNA levels of *IFIT1*, *IFNA1*, *IFNB1* and *TNF* in EP and LP hMPCs.

**(H)** Western blot analysis of STING, p-STING, p-TBK1, p-IRF3 and p-NF-κB protein levels in EP hMPCs transduced with lentiviruses expressing Luc or STING. β-Actin was used as the loading control.

**(I)** Relative mRNA levels of *IFIT1*, *IFNA1*, *IFNB1, ISG15* and *TNF* in EP hMPCs transduced with lentiviruses expressing Luc or STING.

**(J)** Western blot analysis of STING, p-STING, p-TBK1, p-IRF3 and p-NF-κB protein levels in LP hMPCs transfected with si-*STING1*. β-Actin was used as the loading control.

**(K)** Relative mRNA levels of *IFIT1*, *IFNA1*, *IFNB1* and *TNF* in LP hMPCs transfected with si-*STING1*.

**(L)** Western blot analysis of p-STING, p-TBK1, p-IRF3 and p-NF-κB protein levels in LP hMPCs after CRISPRko of *GNPTAB*. β-Actin was used as the loading control.

**(M)** Relative mRNA levels of *IFIT1, IFNA1, IFNB1, ISG15* and *TNF* in LP hMPCs after CRISPRko of *GNPTAB*.

**(N)** ELISA analysis of 2′3′-cGAMP levels in EP hMPCs transduced with lentiviruses expressing Luc or GNPTAB. The 2′3′-cGAMP levels were normalized to 1E5 cells.

**(O)** Schematic diagram summarizing the mechanism by which GNPTAB drives hMPC senescence via activation of the STING innate immune pathway. GNPTAB interacts with STING to activate downstream STING-TBK1-IRF3 signaling axis, which induces SASP and inflammatory responses, thereby driving and amplifying cellular senescence in hMPCs.

Data in all figures except for (D) and (O) are presented as mean ± SEM. Two-tailed unpaired Student's *t* test (A-C, F-N) and one-way ANOVA followed by Tukey's multiple-comparison test (E) were used. $n$ = 3-4 biological replicates in (A)-(C) and (E)-(N).

## Supplementary table legends

Table S1. sgRNAs sequences for LAGs.

Table S2. Enriched genes during LAGs screening in RS hMPCs.

Table S3. DEGs in *GNPTAB*-knockout hMPCs.

Table S4. DEGs in *GNPTAB*-overexpression hMPCs.

Table S5. GNPTAB-interacting proteins identified by Co-IP followed with LC-MS/MS analysis.

Table S6. Primer sequences.

Figure S1

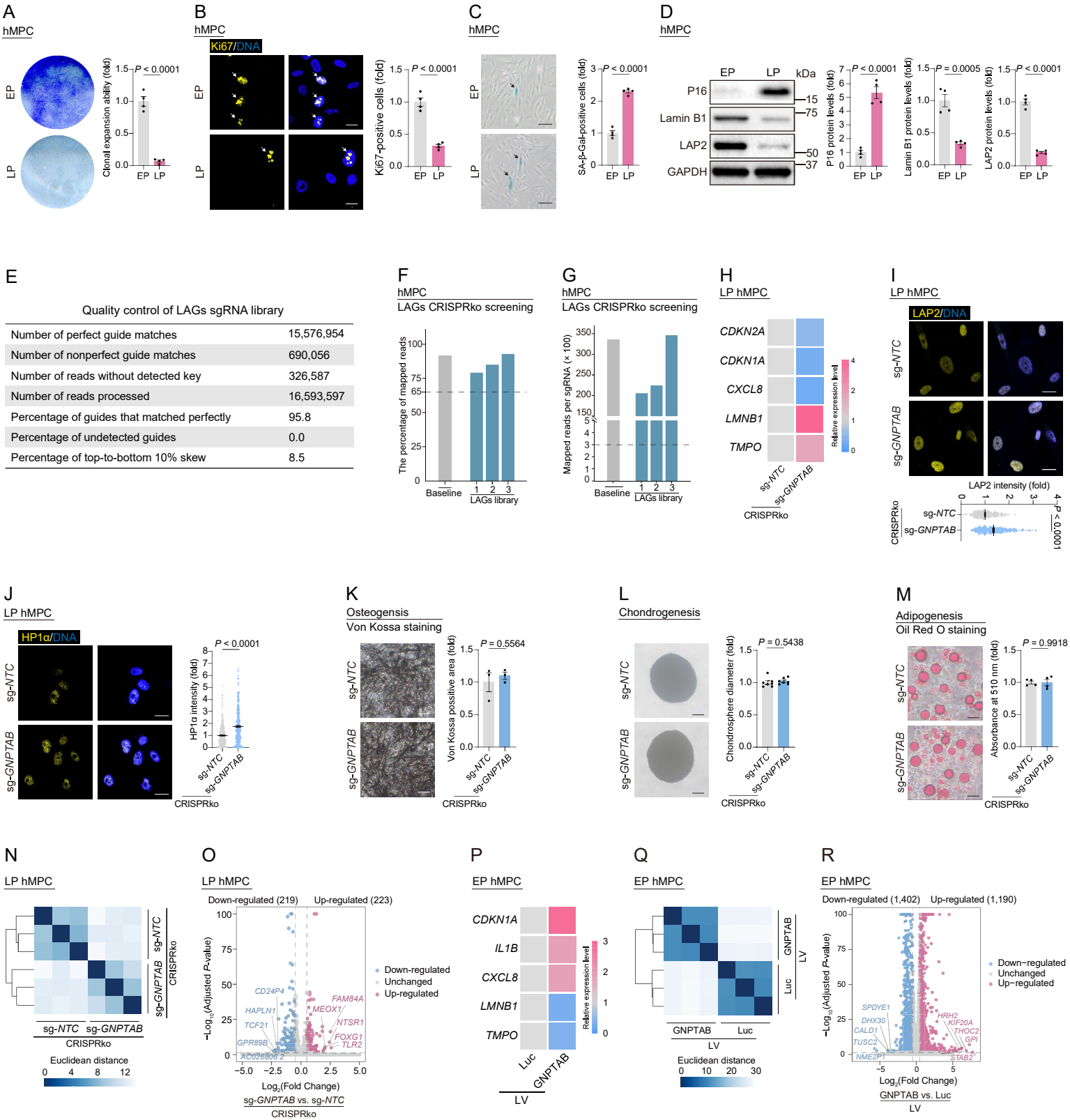
A
hMPC
EP
LP
Clonal expansion ability (fold)
P < 0.0001
B
hMPC
Ki67/DNA
Ki67-positive cells (fold)
P < 0.0001
C
hMPC
SA-β-Gal-positive cells (fold)
P < 0.0001
D
hMPC
EP LP kDa
P16
Lamin B1
LAP2
GAPDH
15
75
50
37
P16 protein levels (fold)
P < 0.0001
Lamin B1 protein levels (fold)
P = 0.0005
LAP2 protein levels (fold)
P < 0.0001
E
Quality control of LAGs sgRNA library
Number of perfect guide matches 15,576,954
Number of nonperfect guide matches 690,056
Number of reads without detected key 326,587
Number of reads processed 16,593,597
Percentage of guides that matched perfectly 95.8
Percentage of undetected guides 0.0
Percentage of top-to-bottom 10% skew 8.5
F
hMPC
LAGs CRISPRko screening
The percentage of mapped reads
Baseline
LAGs library
G
hMPC
LAGs CRISPRko screening
Mapped reads per sgRNA (× 100)
Baseline
LAGs library
H
LP hMPC
CDKN2A
CDKN1A
CXCL8
LMNB1
TMPO
Relative expression level
sg-NTC
sg-GNPTAB
CRISPRko
I
LP hMPC
LAP2/DNA
sg-NTC
sg-GNPTAB
LAP2 intensity (fold)
CRISPRko
P < 0.0001
J
LP hMPC
HP1α/DNA
HP1α intensity (fold)
P < 0.0001
CRISPRko
K
Osteogensis
Von Kossa staining
Von Kossa possitive area (fold)
P = 0.5564
CRISPRko
L
Chondrogenesis
Chondrosphere diameter (fold)
P = 0.5438
CRISPRko
M
Adipogenesis
Oil Red O staining
Absorbance at 510 nm (fold)
P = 0.9918
CRISPRko
N
LP hMPC
sg-NTC
sg-GNPTAB
CRISPRko
Euclidean distance
O
LP hMPC
Down-regulated (219)
Up-regulated (223)
−Log10(Adjusted P-value)
CD24P4
HAPLN1
TCF21
GPR89B
AC026806.2
FAM84A
MEOX1
NTSR1
FOXG1
TLR2
Down-regulated
Unchanged
Up-regulated
Log2(Fold Change)
sg-GNPTAB vs. sg-NTC
CRISPRko
P
EP hMPC
CDKN1A
IL1B
CXCL8
LMNB1
TMPO
Relative expression level
Luc
GNPTAB
LV
Q
EP hMPC
GNPTAB
Luc
LV
Euclidean distance
R
EP hMPC
Down-regulated (1,402)
Up-regulated (1,190)
−Log10(Adjusted P-value)
SPDYE1
DHX30
CALD1
TUSC2
NME2P1
HRH2
KIF20A
THOC2
GPI
STAB2
Down-regulated
Unchanged
Up-regulated
Log2(Fold Change)
GNPTAB vs. Luc
LV

Figure S2

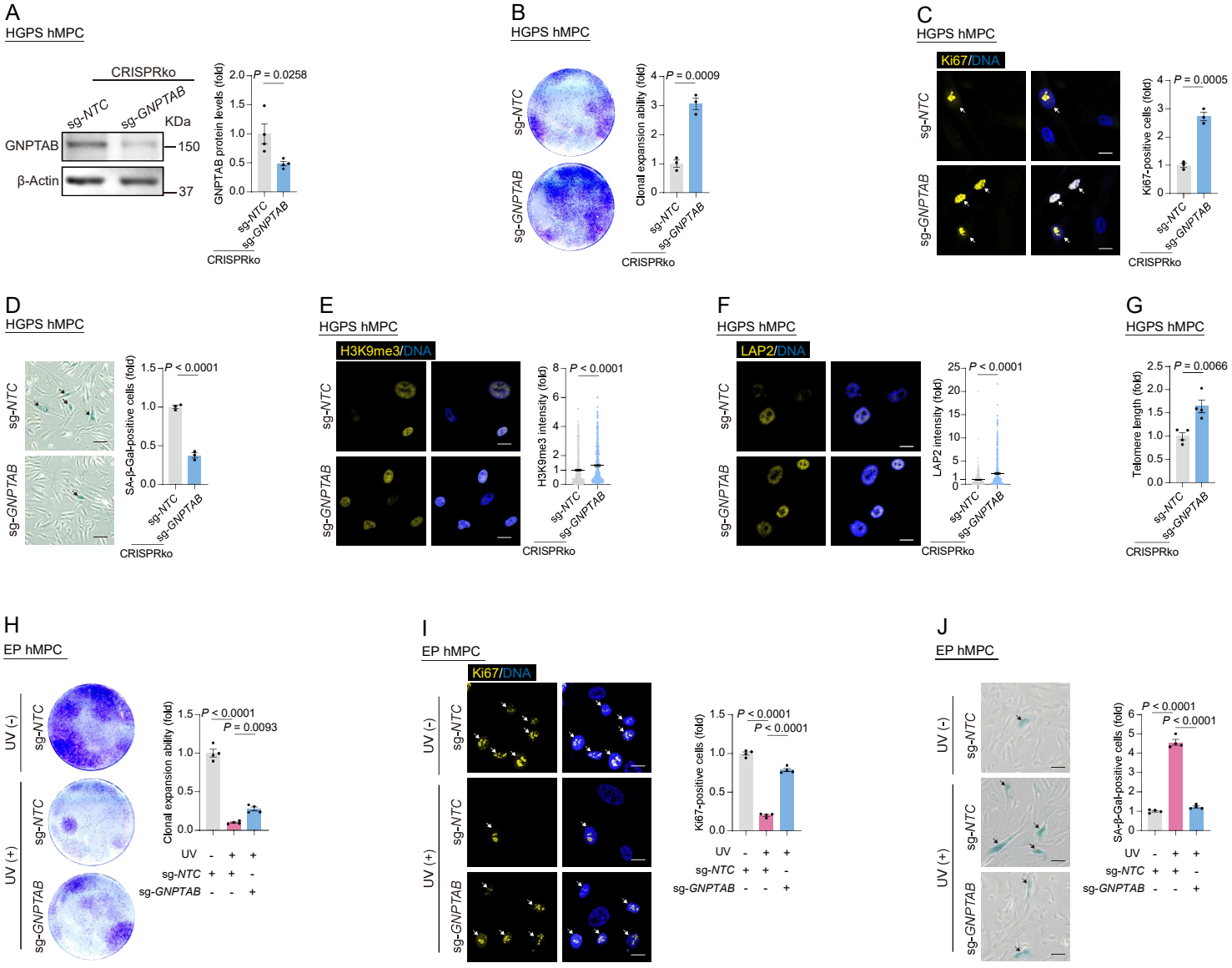
A
HGPS hMPC
CRISPRko
sg-NTC
sg-GNPTAB
KDa
GNPTAB
150
β-Actin
37
GNPTAB protein levels (fold)
P = 0.0258
B
HGPS hMPC
Clonal expansion ability (fold)
P = 0.0009
C
HGPS hMPC
Ki67/DNA
Ki67-positive cells (fold)
P = 0.0005
D
HGPS hMPC
SA-β-Gal-positive cells (fold)
P < 0.0001
E
HGPS hMPC
H3K9me3/DNA
H3K9me3 intensity (fold)
P < 0.0001
F
HGPS hMPC
LAP2/DNA
LAP2 intensity (fold)
P < 0.0001
G
HGPS hMPC
Telomere length (fold)
P = 0.0066
H
EP hMPC
UV (-)
UV (+)
Clonal expansion ability (fold)
P < 0.0001
P = 0.0093
UV
sg-NTC
sg-GNPTAB
I
EP hMPC
Ki67/DNA
Ki67-positive cells (fold)
P < 0.0001
P < 0.0001
J
EP hMPC
SA-β-Gal-positive cells (fold)
P < 0.0001
P < 0.0001

Figure S3

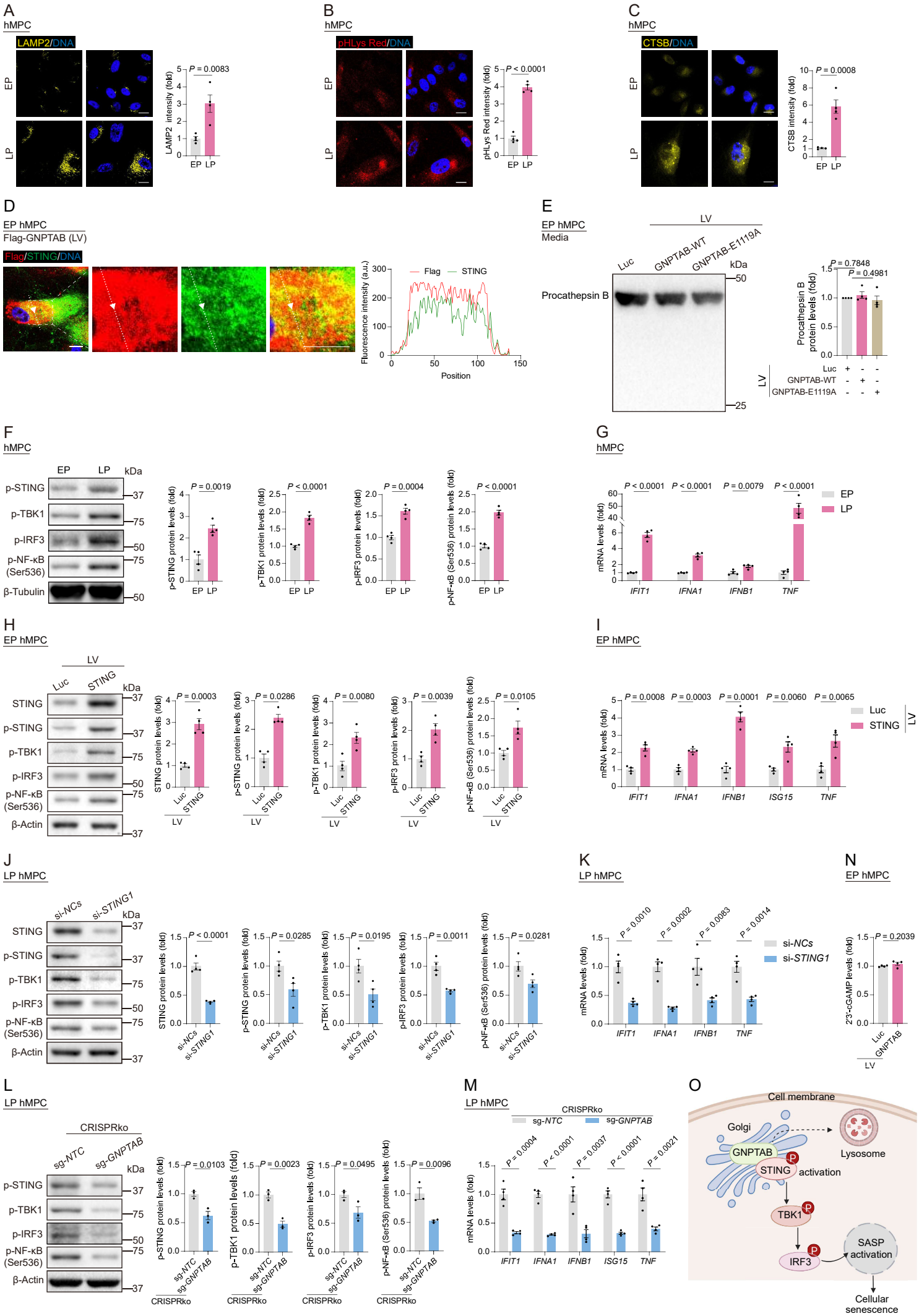
A
hMPC
LAMP2/DNA
EP
LP
LAMP2 intensity (fold)
P = 0.0083
B
hMPC
pHLys Red/DNA
pHLys Red intensity (fold)
P < 0.0001
C
hMPC
CTSB/DNA
CTSB intensity (fold)
P = 0.0008
D
EP hMPC
Flag-GNPTAB (LV)
Flag/STING/DNA
Fluorescence intensity (a.u.)
Flag
STING
Position
E
EP hMPC
Media
LV
Luc
GNPTAB-WT
GNPTAB-E1119A
kDa
Procathepsin B
50
25
Procathepsin B protein levels (fold)
P = 0.7848
P = 0.4981
F
hMPC
EP
LP
kDa
p-STING
p-TBK1
p-IRF3
p-NF-κB (Ser536)
β-Tubulin
37
75
50
75
50
p-STING protein levels (fold)
P = 0.0019
p-TBK1 protein levels (fold)
P < 0.0001
p-IRF3 protein levels (fold)
P = 0.0004
p-NF-κB (Ser536) protein levels (fold)
P < 0.0001
G
hMPC
mRNA levels (fold)
P < 0.0001
P < 0.0001
P = 0.0079
P < 0.0001
IFIT1
IFNA1
IFNB1
TNF
H
EP hMPC
LV
Luc
STING
STING
p-STING
p-TBK1
p-IRF3
p-NF-κB (Ser536)
β-Actin
37
37
75
50
75
37
STING protein levels (fold)
P = 0.0003
p-STING protein levels (fold)
P = 0.0286
p-TBK1 protein levels (fold)
P = 0.0080
p-IRF3 protein levels (fold)
P = 0.0039
p-NF-κB (Ser536) protein levels (fold)
P = 0.0105
I
EP hMPC
mRNA levels (fold)
P = 0.0008
P = 0.0003
P = 0.0001
P = 0.0060
P = 0.0065
IFIT1
IFNA1
IFNB1
ISG15
TNF
Luc
STING
LV
J
LP hMPC
si-NCs
si-STING1
STING
p-STING
p-TBK1
p-IRF3
p-NF-κB (Ser536)
β-Actin
37
37
75
50
75
37
STING protein levels (fold)
P < 0.0001
p-STING protein levels (fold)
P = 0.0285
p-TBK1 protein levels (fold)
P = 0.0195
p-IRF3 protein levels (fold)
P = 0.0011
p-NF-κB (Ser536) protein levels (fold)
P = 0.0281
K
LP hMPC
mRNA levels (fold)
P = 0.0010
P = 0.0002
P = 0.0083
P = 0.0014
IFIT1
IFNA1
IFNB1
TNF
si-NCs
si-STING1
N
EP hMPC
2'3'-cGAMP levels (fold)
P = 0.2039
Luc
GNPTAB
LV
L
LP hMPC
CRISPRko
sg-NTC
sg-GNPTAB
p-STING
p-TBK1
p-IRF3
p-NF-κB (Ser536)
β-Actin
37
75
50
75
37
p-STING protein levels (fold)
P = 0.0103
p-TBK1 protein levels (fold)
P = 0.0023
p-IRF3 protein levels (fold)
P = 0.0495
p-NF-κB (Ser536) protein levels (fold)
P = 0.0096
M
LP hMPC
CRISPRko
sg-NTC
sg-GNPTAB
mRNA levels (fold)
P = 0.0004
P < 0.0001
P = 0.0037
P < 0.0001
P = 0.0021
IFIT1
IFNA1
IFNB1
ISG15
TNF
O
Cell membrane
Golgi
GNPTAB
STING
activation
Lysosome
TBK1
IRF3
SASP activation
Cellular senescence

## References


Dobin A, Davis CA, Schlesinger F et al. STAR: Ultrafast universal RNA-seq aligner. Bioinformatics 2013; 29:15-21.

Geng L, Zhang B, Liu H et al. A comparative study of metformin and nicotinamide riboside in alleviating tissue aging in rats. Life Med 2023; 2:lnac045.

He Y, Ji Q, Wu Z et al. 4E-BP1 counteracts human mesenchymal stem cell senescence via maintaining mitochondrial homeostasis. Protein Cell 2023; 14:202-216.

Jing Y, Jiang X, Ji Q et al. Genome-wide CRISPR activation screening in senescent cells reveals SOX5 as a driver and therapeutic target of rejuvenation. Cell Stem Cell 2023; 30:1452-1471.

Joung J, Konermann S, Gootenberg JS et al. Genome-scale CRISPR-Cas9 knockout and transcriptional activation screening. Nat Protoc 2017; 12:828-863.

Li LZ, Yang K, Jing Y et al. CRISPR-based screening identifies XPO7 as a positive regulator of senescence. Protein Cell 2023; 14:623-628.

Li HY, Wang M, Jiang X et al. CRISPR screening uncovers nucleolar RPL22 as a heterochromatin destabilizer and senescence driver. Nucleic Acids Res 2024; 52:11481-11499.

Li W, Köster J, Xu H et al. Quality control, modeling, and visualization of CRISPR screens with MAGeCK-VISPR. Genome Biol 2015; 16:281.

Li W, Xu H, Xiao T et al. MAGeCK enables robust identification of essential genes from genome-scale CRISPR/Cas9 knockout screens. Genome Biol 2014; 15:554.

Liang R, Arif T, Kalmykova S et al. Restraining lysosomal activity preserves hematopoietic stem cell quiescence and potency. Cell Stem Cell 2020; 26:359-376.

Liao Y, Smyth GK, Shi W. featurecounts: An efficient general purpose program for assigning sequence reads to genomic features. Bioinformatics 2014; 30:923-30.

Liu GH, Barkho BZ, Ruiz S et al. Recapitulation of premature ageing with iPSCs from Hutchinson-Gilford progeria syndrome. Nature 2011; 472:221-5.

Love MI, Huber W, Anders S. Moderated estimation of fold change and dispersion for RNA-seq data with DESeq2. Genome Biol 2014; 15:550.

Sanjana NE, Shalem O, Zhang F. Improved vectors and genome-wide libraries for CRISPR screening. Nat Methods 2014; 11:783-784.

Valdés-Tresanco MS, Valdés-Tresanco ME, Valiente PA et al. gmx_MMPBSA: A New Tool to Perform End-State Free Energy Calculations with GROMACS. J Chem Theory Comput 2021; 17:6281-6291.

Wang W, Zheng Y, Sun S et al. A genome-wide CRISPR-based screen identifies *KAT*7 as a driver of cellular senescence. Sci Transl Med 2021; 13:eabd2655.

Wang B, Wang M, Zhang W et al. Integrative analysis of pooled CRISPR genetic screens using MAGeCKFlute. Nat Protoc 2019; 14:756-780.

Wu Z, Zhang W, Song M et al. Differential stem cell aging kinetics in Hutchinson-Gilford progeria syndrome and Werner syndrome. Protein Cell 2018; 9:333-350.

Yan Y, Zhang D, Zhou P et al. HDOCK: A web server for protein-protein and protein-DNA/rRNA docking based on a hybrid strategy. Nucleic Acids Res 2017; 45:W365-W373.

Zhang S, Wu Z, Shi Y et al. FTO stabilizes MIS12 and counteracts senescence. Protein Cell 2022; 13:954-960.

Zhang W, Li J, Suzuki K et al. Aging stem cells. A Werner syndrome stem cell model unveils heterochromatin alterations as a driver of human aging. Science 2015; 5:1160-3.

Zhang X, Liu Z, Liu X et al. Telomere-dependent and telomere-independent roles of RAP1 in regulating human stem cell homeostasis. Protein Cell 2019; 10:649-667.

Zhou Y, Zhou B, Pache L et al. Metascape provides a biologist-oriented resource for the analysis of systems-level datasets. Nat Commun 2019; 10:1523.